International Journal of Nanomedicine

Dovepress
open access to scientific and medical research

Open Access Full Text Article

ORIGINAL RESEARCH

Hydrophilic mesoporous carbon nanospheres with high drug-loading efficiency for doxorubicin delivery and cancer therapy

This article was published in the following Dove Press journal:
International Journal of Nanomedicine
27 April 2016
Number of times this article has been viewed

Huan Wang[1,2,*]
Xiangui Li[1,*]
Zhiqiang Ma[1]
Dan Wang[3]
Linzhao Wang[1,2]
Jieqiong Zhan[1,4]
Lan She[1]
Feng Yang[1]

[1]Department of Inorganic Chemistry, School of Pharmacy, Second Military Medical University, Shanghai, [2]Department of Pharmacy, Fujian University of Traditional Chinese Medicine, Fuzhou, [3]Department of Obstetrics and Gynecology, Shanghai Changzheng Hospital, Second Military Medical University, Shanghai, [4]Department of Pharmacy, Hebei North University, Zhangjiakou, Hebei, People's Republic of China

*These authors contributed equally to this article

Abstract: In this study, a highly effective transmembrane delivery vehicle based on PEGylated oxidized mesoporous carbon nanosphere (oMCN@PEG) was successfully fabricated in a facile strategy. oMCN@PEG exhibited a narrow size distribution of 90 nm, excellent hydrophilicity, good biocompatibility, and a very high loading efficiency for doxorubicin (DOX). The drug system (oMCN@DOX@PEG) exhibited excellent stability under neutral pH conditions, but with dramatic releases of DOX at reduced pH conditions. Pharmacokinetics study revealed that oMCN@DOX@PEG could prolong the circulation of DOX in the blood stream. The endocytosis, cytotoxicity, and anticancer effect in vitro and in vivo of the drug-loaded nanoparticles were also evaluated. Our results showed that the nanoparticles efficiently penetrated the membrane of tumor cells, subsequently released drugs, and efficiently inhibited the growth of cancer cells both in vitro and in vivo. Especially, oMCN@DOX@PEG also exhibited significant antimetastasis effect in advanced stage of malignant cancer, improving the survival time of tumor-bearing mice. The results suggested that oMCN@PEG might be a promising anticancer drug delivery vehicle for cancer therapy.

Keywords: drug delivery, hydrophilic, mesoporous carbon nanoparticles, tumor metastasis

Introduction

Chemotherapy is one of the most effective methods for cancer treatments. However, the nonselective destruction to normal cells has greatly limited the application of anticancer drugs. Construction of delivery system is of great importance in enhancing the efficacy and reducing the side effect of anticancer drugs. Recently, ordered mesoporous nanoparticles, especially the well-known mesoporous silica nanoparticles, have attracted increasing attention due to their remarkable properties such as large surface area, large pore volume, and uniform mesoporous structures. These features make them ideal platforms in the drug delivery system (DDS).[1–3] By contrast, mesoporous carbon nanoparticles (MCNs) are more suitable to load hydrophobic drugs with high loading efficiency through π-stacking and/or hydrophobic interaction with carbonaceous framework.[4,5] In addition, MCNs with suitable size can be easily uptaken by tumor cells.[6,7] All these make MCNs promising materials in transmembrane delivery and stimuli-responsive releasing vehicles.

However, quite limited research has been reported to employ MCNs as effective carriers for DDS due to the following difficulties. First, ordered mesoporous carbons prepared by conventional methods usually have irregular morphology and large size (>1 μm), which cannot be effectively uptaken by most tumor cells.[8] Second, the hydrophobic

Correspondence: Feng Yang; Lan She
Department of Inorganic Chemistry, School of Pharmacy, Second Military Medical University, 325 Guohe Road, Shanghai 200433, People's Republic of China
Tel +86 21 8187 1218
Email yangfeng1008@126.com; slgs4100@126.com

submit your manuscript | www.dovepress.com
Dovepress
http://dx.doi.org/10.2147/IJN.S103020

nature makes MCNs poorly dispersed in water under physiological condition. They tend to aggregate and sedimentate in blood stream, not to mention the ability of long circulation time. Third, the biocompatibility of carbon-based materials is always controversial. In some researches on carbon nanodots, good biocompatibility has been achieved.[9] However, other research showed that carbon nanotubes or graphenes could activate the complement system or induce immunotoxicity to some extent.[10,11] So it is a great challenge to prepare hydrophilic and biocompatible MCNs as nanoplatforms for the delivery and release of anticancer drugs.

Herein, we have succeeded in establishing a DDS based on MCNs with uniform morphology, suitable diameter, excellent hydrophilicity, and good biocompatibility. As shown in Figure 1, we first synthesized MCNs with spherical morphology and a diameter of 90 nm through a low-concentration hydrothermal treatment based on previous work.[12] To improve the hydrophilicity of MCNs, we introduced large amounts of oxygen-containing groups (typically hydroxyl or carboxyl groups) onto the surface of MCNs by hydrogen peroxide under mild oxidization treatments. So the oxidized MCNs were synthesized and named as oMCNs. Then, the anticancer drug doxorubicin (DOX) was loaded in the vehicles. Finally, PEGylated phospholipid DSPE-mPEG2000, a recognized biocompatible material, was employed as a protective layer on the outer surface of the drug-loaded nanoparticles. As expected, the PEGylated oxidized oMCN (oMCN@PEG) will be a promising carrier with high drug-loading efficiency and effective delivery of DOX molecules into tumor cells, consequently killing them at low dose and with significantly reduced side effects.

Material and methods

Reagents and materials

Pluronic F127 ($PEO_{106}PPO_{70}PEO_{106}$) was purchased from BASF Co., Ltd (Hanover, Germany). DSPE-mPEG2000 was purchased from Avanti Polar Lipids, Inc (Alabaster, AL, USA). DOX and fluorescein isothiocyanate were supplied by Dalian Meilun Biology Co. Ltd (Dalian, People's Republic of China). Other chemical reagents, such as phenol, formalin aqueous solution, NaOH, hydrogen peroxide, and chloroform, were purchased from Shanghai Chemical Regent Co (Shanghai, People's Republic of China). The Dulbecco's Modified Eagle's Medium (DMEM), culture medium, fetal bovine serum (FBS), and Cell Counting Kit-8 (CCK-8) were obtained from Thermo Fisher Scientific (Waltham, MA, USA).

Cell lines and animals

Lewis lung carcinoma (LLC) cell lines were presented by Institute of Immunology, Second Military Medical University (Shanghai, People's Republic of China) after approval by the Institutional Review Board of Second Military Medical

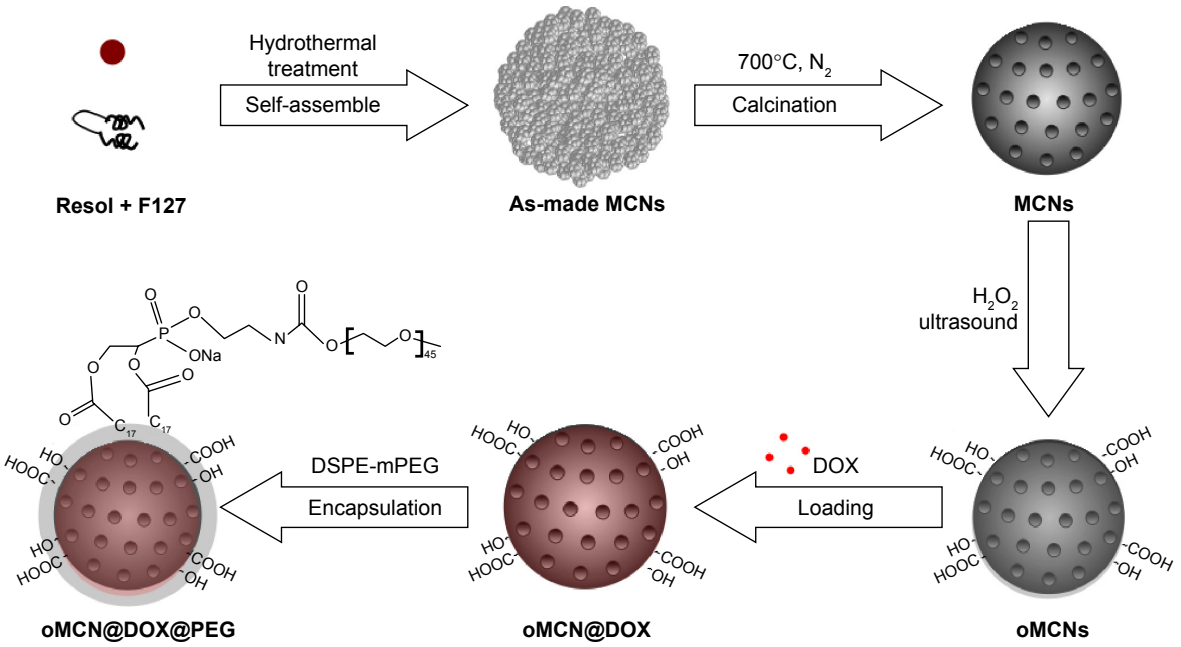

Figure 1 A schematic illustration for the synthesis, drug loading, and surface modification of nanoparticles.
Abbreviations: MCNs, mesoporous carbon nanospheres; oMCN@DOX@PEG, polyethylene glycol-modified doxorubicin-loaded oxidized mesoporous carbon nanospheres; DSPE-mPEG, 1,2-distearoyl-sn-glycero-3-phosphoethanolamine-N-(methoxy[polyethylene glycol]-2000); oMCN@DOX, doxorubicin-loaded oxidized mesoporous carbon nanospheres; DOX, doxorubicin; oMCNs, oxidized mesoporous carbon nanospheres.

University. Male C57BL/6N mice (6–8 weeks) and Sprague Dawley rats (male, 200±20 g) were purchased from the Animal Experimental Center of Second Military Medical University. All animal experiments were performed in compliance with the Guiding Principles for the Care and Use of Laboratory Animals, Second Military Medical University, People's Republic of China.

Synthesis and surface modification of MCNs

In this study, MCNs were synthesized through a low-concentration hydrothermal approach according to the literature[12] with some modification. In brief, 0.6 g of phenol, 2.1 mL of formalin aqueous solution (37 wt%), and 15 mL of NaOH aqueous solution (0.1 M) were mixed and stirred at 70°C for 0.5 hours to obtain low-molecular-weight phenolic resole resins. After that, 0.96 g of triblock copolymer F127 dissolved in 65 mL of H_2O was added. Then, the mixture was stirred at 66°C at a stirring speed of 340±40 rpm for 16–18 hours. In all, 35 mL of the obtained solution diluted with 112 mL of H_2O was transferred into an autoclave and heated at 130°C for 24 hours. The MCNs were obtained after carbonization at 700°C in the N_2 atmosphere for 3 hours.

A total of 100 mg of the obtained MCNs was dispersed in 50 mL of hydrogen peroxide solution by ultrasound treatment for 4 hours at room temperature. After that, the oxidized MCNs denoted as oMCNs were collected after cycles of centrifugation and washed for three times. At last, the oMCNs were obtained after drying at 100°C in an oven. MCNs treated with nitrite acid solution (5 M) in a similar way were prepared as control.

Optimization of drug-loading procedure

DOX loading was performed by simply mixing DOX solution with oMCNs or MCN suspension. The influence of pH values and weight ratio between DOX and oMCNs were also investigated. In a typical procedure, 10 mg of oMCNs was dispersed in 12 mL of phosphate-buffered saline (PBS) at pH 9.0 under ultrasound assistance. Then, 8 mL of 5 mg/mL DOX aqueous solution was dropped into the dispersion slowly. The mixture was further treated with ultrasound for 30 minutes and then stirred at room temperature under dark condition for 24 hours. The formed complex (denoted as oMCN@DOX) was collected by repeated ultracentrifugation (12,000 rpm, 10 minutes) with PBS at pH 9.0 until the supernatant became clear or reddish. All the unbounded DOX in solution was collected and calculated by measuring the absorbance at 494 nm (characteristic absorbance of DOX) with a UV–Vis absorption spectrophotometer. The drug-loading efficiency here is defined as the ratio of the dosage of DOX loaded onto the nanoparticles and the dosage of the DOX-loaded nanoparticles.

Encapsulation of DSPE-mPEG

In all, 20 mg of the oMCN@DOX was dispersed in the chloroform solution (30 mL, 1 mg/mL) of DSPE-mPEG2000 under ultrasound assistance and stirred for another 4 hours. The mixture was rotary evaporated slowly in vacuum for 3 hours to remove the solvents and then dialyzed against deionized water for 24 hours to remove the residual DSPE-mPEG2000. The oMCN@DOX@PEG was obtained after lyophilization for 24 hours. The oMCN@PEG was prepared similarly but without the addition of DOX.

In vitro release profile examination

The in vitro release profile of DOX from oMCN@DOX@PEG under different pH conditions was examined by a dialysis method in PBS (pH 5.5 or 7.4) at 37°C. Briefly, 2 mg of oMCN@DOX@PEG was encapsulated into a dialysis bag (molecular weight cut off [MWCO] 5,000 Da) and immersed in 50 mL of release medium under stirring at 100 rpm. At interval time point, 1 mL of sample was collected and replaced with an equal volume of fresh medium. The amount of DOX in dialysate was collected for quantitative analysis by UV–Vis spectroscopy after filtration through a 0.22 μm membrane filter.

Characterization techniques

Small-angle X-ray diffraction (SAXS) measurements were taken on a Nanosat U SAXS system (Bruker Optik GmbH, Ettlingen, Germany) using $Co_{ok\alpha}$ radiation (40 kV, 35 mA). Transmission electron microscopy experiments were conducted using a Philips CM200 (Philips, Amsterdam, the Netherlands) microscope operated at 200 kV. The samples for TEM measurements were suspended in ethanol and dropped onto a holey carbon film supported on a Cu grid. Nitrogen adsorption/desorption isotherms were measured at −196°C with a TriStar 3000 analyzer (Micromeritics, Atlanta, GA, USA). The Brunauer–Emmett–Teller equation was used to calculate the apparent surface area from adsorption data obtained at P/P_0 between 0.05 and 0.2. The total volume of micro- and mesopores was calculated from the amount of nitrogen adsorbed at P/P_0=0.95, assuming that adsorption on the external surface was negligible when compared to adsorption in pores. The pore size distributions were calculated by analyzing the adsorption branch of the N_2 sorption

isotherm using the Barrett–Joyner–Halenda method. Laser Raman spectroscopy was carried out with a LabRAM-1B spectrometer (Paris, France). Fourier transform infrared (FTIR) spectra were measured in the range of 400–4,000 cm^{-1} using an Avatar 370 spectrometer (Nicolet Madison, AL, USA). The size distribution and zeta potential of particles were measured at 20°C by a Nanosizer ZS-90 (Malvern Instruments, Malvern, UK).

Membrane permeability and intracellular release

LLC cells were grown in DMEM supplemented with 10% FBS at 37°C and 5% CO_2. Then 5×10^5 cells were seeded on 14 mm glass coverslips in a chamber and allowed to adhere overnight. After incubation with oMCN@DOX@PEG or free DOX at 37°C under 5% CO_2, the cells were fixed with 4% paraformaldehyde and their nuclei were stained with 4′, 6′-diamidino-2-phenylindole (5 μg/mL). The cells were washed several times with sterilized PBS before being analyzed by fluorescence microscopy (IX 71; Olympus Corporation, Tokyo, Japan) and a charge-coupled device (Cascade 650; Olympus Corporation, Tokyo, Japan).

Cytotoxicity

Cell viability was determined by CCK-8 assay. LLC cells were seeded into 96-well plates at a concentration of 5×10^4/mL in DMEM supplemented with 10% FBS. After incubation for 24 hours at 37°C under 5% CO_2 atmosphere, the cells were exposed to DOX, oMCN@DOX@PEG, and oMCN@PEG at different concentrations. After 24–48 hours of incubation, the media were removed and the attached cells were washed with PBS. Then 10% of CCK-8 reagent was added for 2 hours at 37°C under 5% CO_2 atmosphere. The absorbance was monitored at 450 nm on a microplate reader (ELx800; BioTek, Winooski, VT, USA). Culture medium without the addition of nanoparticles was used as the blank control. The cytotoxicity was expressed as the percentage of the cell viability when compared with the blank control.

Cell apoptosis

1×10^5 LLC cells were seeded into each well of a 24-well plate. After treatments with oMCN@DOX@PEG and oMCN@PEG, LLC cells were doubly stained with Annexin V and propidium iodide (PI) following manufacturer's instruction. Samples were examined by fluorescence-activated cell sorter analysis, and the results were analyzed using CellQuest software (Becton Dickinson, San Jose, CA, USA).

Pharmacokinetics

Eighteen Sprague Dawley rats (male, 200±20 g) were randomly assigned to three groups (six rats per group). Free DOX, oMCN@DOX nanoparticles, or oMCN@DOX@PEG nanoparticles were injected intravenously with a single dose (8 mg/kg DOX) via tail vein. At different time points, 500 μL of blood samples were collected from retro-orbital sinus and immediately centrifuged to collect the plasma fraction. All plasma samples were pretreated as follows: 100 μL of plasma was spiked with 50 μL of internal standard (daunorubicin, 1.0 μg/mL in methanol) and 400 μL of acetonitrile and vortexed for 5 minutes. The supernatant was collected and evaporated under nitrogen flow at room temperature, and the residual was dissolved in 100 μL of methanol for high-performance liquid chromatography analysis. Plasma concentrations of DOX were determined using a high-performance liquid chromatography system (Agilent Technologies, Santa Clara, CA, USA) equipped with a Symmetry C-18 column (4.6 mm ×150 mm, 5 μm; Waters, San Antonio, TX, USA). The mobile phase was composed of 50:50 (*V*/*V*) A/B, where A was 1.44 g of lauryl sodium sulfate and 0.68 mL of phosphoric acid in 500 mL of water containing 60 mL of methanol and B was acetonitrile. The flow rate was 1.0 mL/min. The detection wavelength was at 233 nm. Pharmacokinetics parameters were calculated using the DAS 2.0 software. (Mathematical Pharmacology Professional Committee of China, Shanghai, People's Republic of China).

In vivo antitumor assays

The LLC tumor-bearing model was established in male C57BL/6N mice. These mice were inoculated subcutaneously in the right posterior limb area with LLC (1×10^6). When the tumor size was ~5 mm ×5 mm in a week, the tumor-bearing mice were randomly divided into three groups (n=6). Treatments consisted of free DOX, oMCN@DOX@PEG, and saline. All the groups were injected via the tail vein. The dose of DOX in each formulation was 2.5 mg/kg/mouse. All the groups were treated on days 0, 3, 6, 9, 12, and 15. Tumor volumes, body weight, and survival time were observed. Tumor volumes were calculated according to the formula $V=0.5a\times b^2$, where a was the largest superficial diameter and b was the smallest superficial diameter. To detect the pulmonary metastasis, another three mice in each group were sacrificed on days 19, 22, and 25 after the implantation of LLC cells. The metastatic foci of the lungs were quantified in each group under the dissecting microscope.

Ex vivo fluorescence imaging assays

To analyze the in vivo distribution of the nanoparticles, C57BL/6N mice were inoculated intramuscularly in the right posterior limb area with LLC (1×10^6). When the volume of tumors reached ~400 mm^3, mice were randomly assigned to three groups: 1) saline (control); 2) free DOX solution; and 3) oMCN@DOX@PEG with 5 mg/kg of DOX each mouse. All mice were administered with the formulations via intravenous injections (tail vein). After 12 hours, the mice were sacrificed and tumors as well as organs were excised from the mice. The fluorescence images of the tumors and organs were taken with a MAESTRO in vivo imaging system (Maestro™; Cri, Woburn, MA, USA).

Statistical analysis

All the data in this study were analyzed by the statistic package SPSS 18.0 (SPSS Inc., Chicago, IL, USA). Data were expressed as mean ± standard deviation (SD). For values that were normally distributed, direct comparison between two groups was conducted by independent samples *t*-test. *P*-values <0.05 were considered statistically significant.

Results and discussion

Synthesis and characterization of oMCNs and oMCN@PEG

As illustrated in Figure 1, the MCNs were first synthesized by using Pluronic F127 as a structure-directing agent and phenolic resol as a carbon resource. A low-concentration hydrothermal treatment was carried out to promote the assembly process. After calcination at 700°C in the N_2 atmosphere, the MCNs were obtained. In order to improve the hydrophilicity, we intended to introduce hydrophilic groups onto the surface of MCNs. Significant efforts have been devoted to the surface functionalization of carbon materials, and wet oxidation treatment is one of the most convenient and simplest methods.[13] Though it has been widely reported that nitric acid oxidation can attach large amounts of oxygen-containing groups to the carbon surface, structural collapse of the ordered framework might happen inevitably during the harsh oxidation condition.[14] Therefore, we chose hydrogen peroxide solution as the mild oxidant to introduce hydrophilic groups onto the surface of the MCNs. After loading with DOX, the oMCN@DOX was subsequently wrapped up by DSPE-mPEG2000 with hydrophobic segments physically absorbed on the surface of the oMCNs and hydrophilic parts as the outer layers, which helped to avoid the recognition of reticuloendothelial system.[15–17]

In order to confirm that hydrophilic groups and polyethylene glycol were successfully introduced to the MCNs, the FTIR and ^{1}H-nuclear magnetic resonance spectra were collected, as shown in Figure 2. From the FTIR spectra (Figure 2A), it can be clearly seen that the MCNs exhibited typical related absorption bands of aromatic hydrocarbons at 2,025 cm^{-1}, 1,630–1,530 cm^{-1}, 1,130 cm^{-1}, and 693–561 cm^{-1}, corresponding to conjugated C=C stretching vibration, aromatic rings skeleton stretching vibration, and in-plane and out-of-plane C–H bending vibrations, respectively, while the oMCNs and oMCN@PEG exhibited absorption bands at 3,438 cm^{-1}, 1,722 cm^{-1}, and 1,190 cm^{-1}, corresponding to –OH, C=O, and =C–O stretching vibrations. In addition, the oMCN@PEG showed typical absorption bands of -CH_3, -CH_2, and C-O at 2,917–2,850 cm^{-1} and 1,110 cm^{-1}.

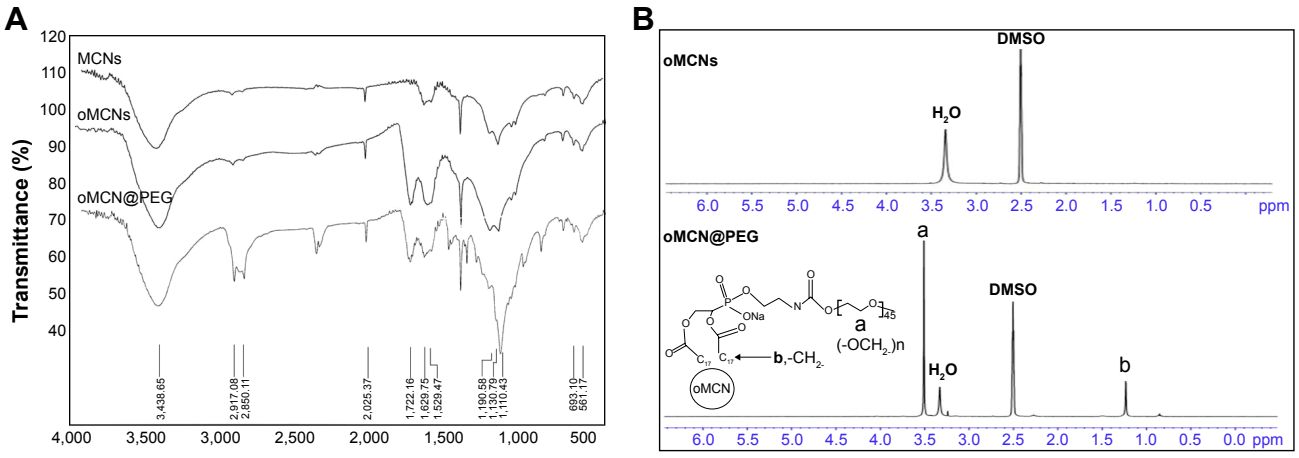

Figure 2 Characterizations of functional groups.

Notes: (**A**) FTIR spectra of MCNs, oMCNs, and oMCN@PEG. (**B**) ^{1}H-NMR spectra of oMCNs and oMCN@PEG in DMSO-d_6.

Abbreviations: FTIR, Fourier transform infrared; MCNs, mesoporous carbon nanospheres; oMCNs, oxidized mesoporous carbon nanospheres; oMCN@PEG, polyethylene glycol-modified oxidized mesoporous carbon nanospheres; ^{1}H-NMR, ^{1}H-nuclear magnetic resonance; DMSO, dimethylsulfoxide.

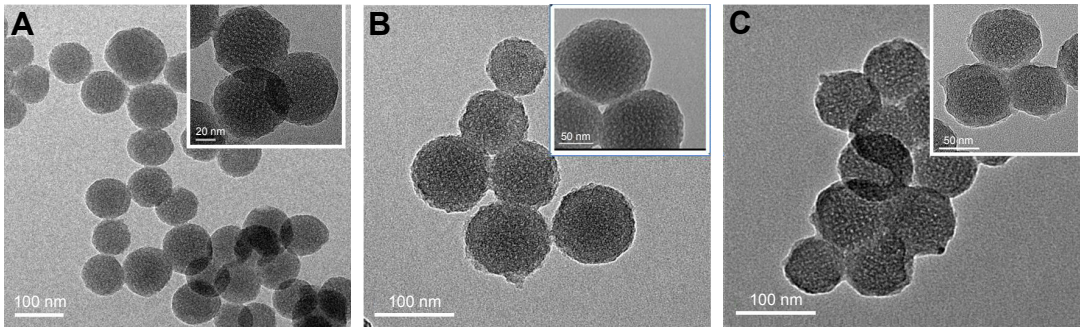

Figure 3 TEM images of nanoparticles.
Notes: (**A**) MCNs, insert HRTEM of MCNs; (**B**) oMCNs, insert HRTEM of oMCNs; and (**C**) oMCN@PEG, insert HRTEM of oMCN@PEG.
Abbreviations: TEM, transmission electron microscope; MCNs, mesoporous carbon nanospheres; HRTEM, high-resolution transmission electron microscopy; oMCNs, oxidized mesoporous carbon nanospheres; oMCN@PEG, polyethylene glycol-modified oxidized mesoporous carbon nanospheres.

So the results of FTIR spectra showed that we had succeeded in synthesizing oMCN@PEG. ^{1}H-nuclear magnetic resonance spectra (Figure 2B) also showed similar results. The oMCNs exhibited solvent peaks at 2.5 ppm and 3.34 ppm only, while the oMCN@PEG exhibited characteristic peaks of H of polyethylene glycol at 1.23 ppm and 3.51 ppm additionally.

The morphology and mesostructure of nanoparticles were characterized by TEM (Figure 3A–C). It was found that the MCNs had spherical morphology, uniform diameter of ~90 nm, and well-defined mesoporous structure. The mesoporous size roughly measured was ~3 nm from the high-resolution transmission electron microscopy images (Figure 3A). The oMCN samples also displayed spherical morphology and a relative monodispersed size distribution of 95 nm. A layer of ~5 nm thick shell coated on the oMCNs could be indistinctly observed (Figure 3C), which consisted of DSPE-mPEG2000.

The SAXS pattern of the MCNs and oMCNs both showed two resolved scattering peaks with q ratio values of $1:\sqrt{3}$, which can be indexed as the 110 and 211 reflections of a body-centred cubic $Im\bar{3}m$ mesostructure (Figure 4A). The results also indicate that MCNs maintained the

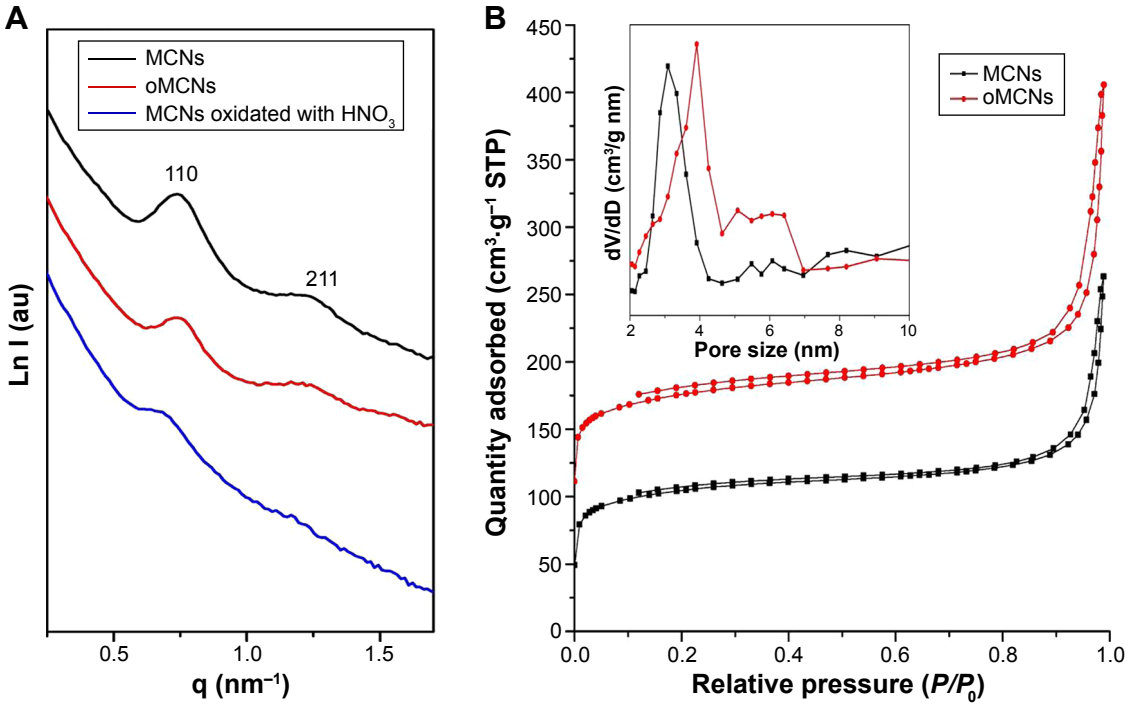

Figure 4 Structure analysis of samples.
Notes: (**A**) SAXS patterns and (**B**) nitrogen adsorption–desorption isotherms, insert pore size distribution curves of the samples. "q" refers to scattering vector.
Abbreviations: SAXS, small-angle X-ray scattering; MCNs, mesoporous carbon nanospheres; oMCNs, oxidized mesoporous carbon nanospheres; au, arbitrary unit; STP, standard temperature and pressure; Ln I, natural logarithm of intensity.

Table 1 Structure parameters for the synthesized MCNs and oMCNs samples

Samples	Cell parameter, *a* (nm)[a]	BET surface area ($m^2 \cdot g^{-1}$)[b]	Pore volume ($cm^3 \cdot g^{-1}$)	Pore size (nm)[c]
MCNs	12.0	710	0.55	3.1
oMCNs	12.0	648	0.63	3.9

Notes: [a]Calculated from the SAXS results. [b]Calculated by the multipoint BET model from the adsorption data. [c]Calculated by the BJH model from the adsorption branches of the isotherms.
Abbreviations: MCNs, mesoporous carbon nanospheres; oMCNs, oxidized mesoporous carbon nanospheres; BET, Brunauer–Emmett–Teller; SAXS, small-angle X-ray scattering; BJH, Barrett–Joyner–Halenda.

structural order during surface oxidation with hydrogen peroxide. However, the ordered framework was severely damaged by HNO_3 treatment by contrast as the scattering peaks weakened significantly. N_2 adsorption–desorption analysis was used to tract the pore structure evolvement (Figure 4B), and the structure parameters of MCNs and oMCNs are summarized in Table 1. The pore size and pore volume of oMCNs were somewhat enlarged, while the specific surface reduced after the oxidation treatment with hydrogen peroxide.

MCNs exhibited an average hydrodynamic diameter of 94.8 nm determined by dynamic light scattering (Figure 5A). After oxidation with hydrogen peroxide and conjugation with DSPE-mPEG, the hydrodynamic diameters became 102.2 nm and 108 nm, respectively, slightly larger than before. In addition, hydrogen peroxide introduced large amounts of oxygen-containing groups to the MCNs, causing surface zeta potential to sharply descend from −3.4 mV to −45 mV. The surface zeta potential of the oMCN@PEG was −33.4 mV due to charge screening of DSPE-mPEG2000 (Figure 5B). Owing to the hydrophobic nature of carbon materials, the MCNs were hard to disperse in PBS. Once stirring or ultrasound assistance was withdrawn, the MCNs would deposit within several seconds as indicated visually in Figure 5C. While after surface modification, the suspendability of oMCN@PEG was remarkably improved, making it possible for administration of drugs. The results also suggested the successful surface modification of the MCNs.

Drug loading and release

DOX is a first-line anticancer drug and widely applied in clinic. We chose it as the model drug in this work not only for its specific pesticide effect but also for its unique molecule structure. The aromatic groups of DOX molecules can strongly interact with graphene plate of carbon framework via supramolecular π–π stacking and hydrophobic interactions.[4,5,18] The Raman spectra (Figure 6A) showed

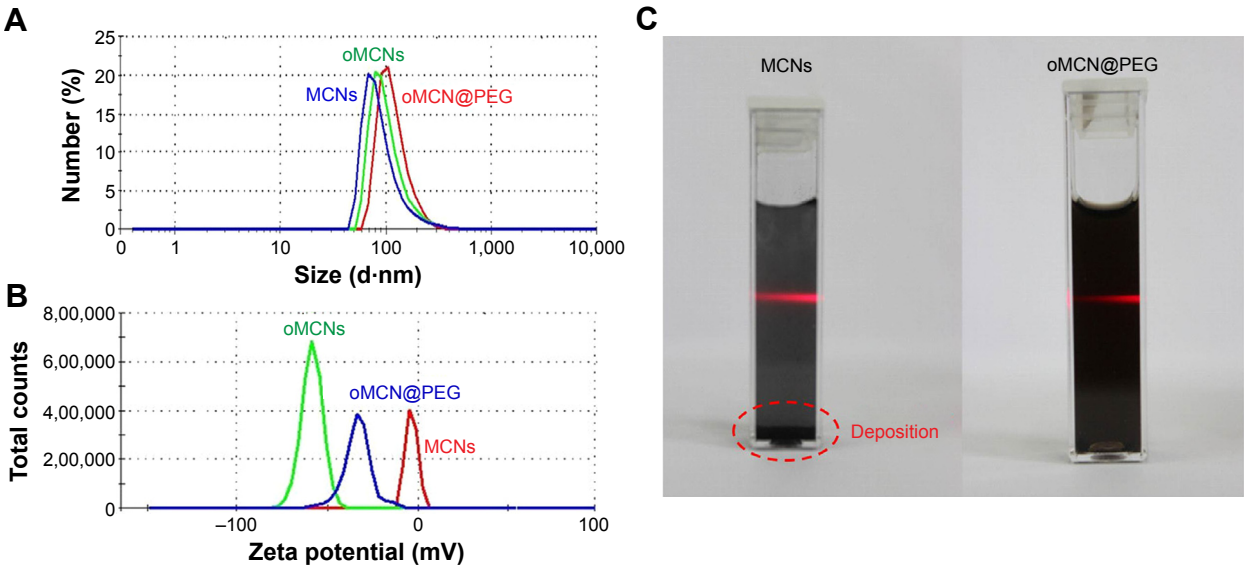

Figure 5 Typical DLS profile of nanoparticles measured in aqueous solution.
Notes: (**A**) Hydrodynamic diameters. (**B**) Zeta potential measurements of nanoparticles. (**C**) Photos of MCNs and oMCN@PEG redispersed in PBS with Tyndall phenomenon.
Abbreviations: DLS, dynamic light scattering; MCNs, mesoporous carbon nanospheres; oMCNs, oxidized mesoporous carbon nanospheres; oMCN@PEG, polyethylene glycol-modified oxidized mesoporous carbon nanospheres; PBS, phosphate buffer solution.

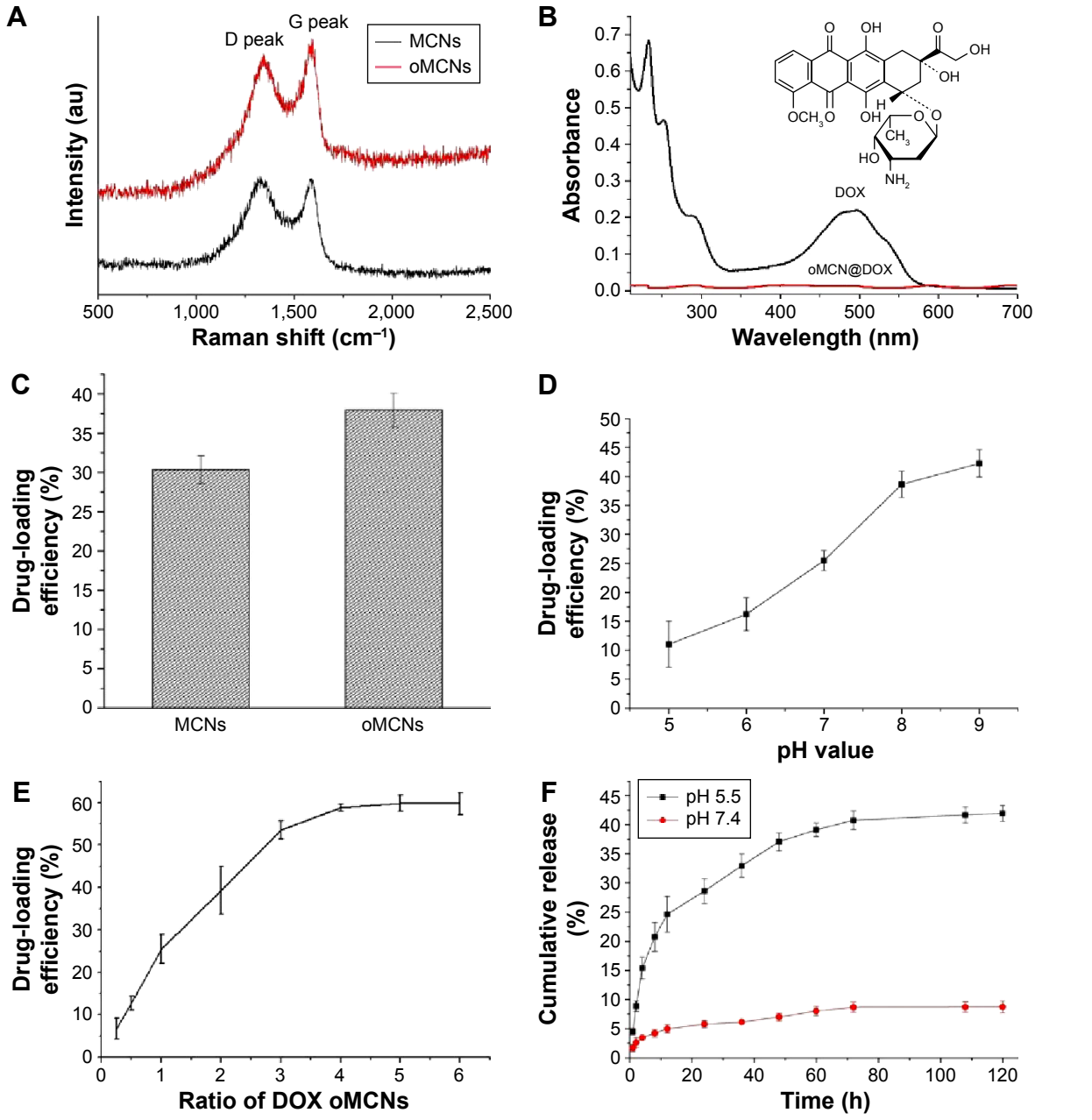

Figure 6 Drug loading and release process.

Notes: (**A**) Raman spectra of MCNs before and after oxidation. (**B**) UV–Vis spectra of free DOX and oMCN@DOX; structure of DOX is insert. Comparison of drug-loading efficiency of (**C**) MCNs before and after modification, (**D**) different pH values of PBS, and (**E**) different weight ratios of DOX to oMCNs. (**F**) Release profile of oMCN@DOX@PEG against different pH values.

Abbreviations: MCNs, mesoporous carbon nanospheres; UV–Vis, ultraviolet visible; DOX, doxorubicin; oMCN@DOX, doxorubicin-loaded oxidized mesoporous carbon nanospheres; pH, potential of hydrogen; PBS, phosphate buffer solution; oMCNs, oxidized mesoporous carbon nanospheres; oMCN@DOX@PEG, polyethylene glycol-modified doxorubicin-loaded oxidized mesoporous carbon nanospheres; au, arbitrary unit; h, hours.

a structure of graphite with defects of MCNs before and after oxidation according to the presence of typical D peak and G peak at Raman shift of 1,343 cm^{-1} and 1,585 cm^{-1}, respectively. The representative absorption peak of DOX almost disappears in oMCN@DOX solution, indicating the successful loading of DOX molecules into the mesopores of oMCNs (Figure 6B). oMCNs had a higher loading efficiency than MCNs because oMCNs have larger pore size and pore volume than MCNs (Figure 6C). The amino group also played an important role in the drug-loading process. When the pH values of solution were acidic, the DOX became more hydrophilic owing to the protonation of the amino group. In contrast, the DOX became more hydrophobic in mild base, which benefited drug loading

(Figure 6D). The suitable ratio of DOX to oMCNs was 4:1 as could be seen from Figure 6E. All these reasons mentioned earlier as well as the low density of carbon contributed to a drug-loading efficiency of as high as 59.7%±2.6% under the optimum condition. As far as we know, there have been a few nanocarriers that have such high drug-loading efficiency.[19–22] The oMCNs showed a significant advantage as containers for DOX.

Analogously, we found that the amount of DOX released from oMCN@DOX@PEG was pH dependent (Figure 6F). In neutral environment, only ~8.7% of DOX was released over 120 hours. By contrast, ~42% of total DOX was released over 72 hours in the acid medium because of the protonation of the amino group, as we know that the microenvironments of extracellular tissues of tumors are acidic. The pH values of intracellular lysosomes and endosomes are even lower.[23,24] The pH-dependent drug release from this delivery system potentially facilitated active drug accumulation in tumor tissues and reduced the toxicity to normal tissues.

Membrane permeability and intracellular release

We further investigated the transmembrane delivery and intracellular release processes of oMCN@DOX@PEG by fluorescent images because the DOX can emit a red light under an excitation of 532 nm. After incubation with 10 μg/mL of oMCN@DOX@PEG for 1 hour, as clearly depicted in Figure 7A–D, a great number of nanoparticles were uptaken by LLC cells and formed aggregates in the cytoplasm, easy to reach the lethal concentration with very high drug-loading efficiency by each nanoparticle. To investigate the property of intracellular release, we incubated the LLC cells with oMCN@DOX@PEG for 0.5 hours, 1 hour, and 2 hours. As shown in Figure 7E–G, the fluorescence intensity of LLC cells was higher as time extended, which indicated that DOX molecules began to release from oMCN@DOX@PEG. As comparison, LLC cells were incubated with the same amount of free DOX for 1 hour and the fluorescence was much weaker (Figure 7H). The results imply that oMCN@PEG can be used as transmembrane delivery vehicles for intracellular release of drugs.

Biocompatibility of oMCN@PEG and cytotoxicity of oMCN@DOX@PEG

To evaluate the biocompatibility of the synthesized oMCN@PEG, the cell viability was further measured by the CCK-8 assays (Figure 8). Fibroblast cells of L929 and tumor cells of Hela and LLC were incubated with oMCN@PEG at different concentrations for 24 hours or 48 hours. No obvious growth inhibition was found at concentration <12.5 μg/mL for the three cell lines (Figure 8A–C). Even the oMCN@PEG concentration was high up to 100 μg/mL, ~67% L929 cells still survived after 48 hours of incubation. Since Hela cells and LLC cells are generally more tolerant than normal cells, ~76% Hela and 71% LLC cells still survived with 100 μg/mL of the oMCN@PEG after 48 hours of incubation. These results indicated that oMCN@PEG has very good biocompatibility in vitro.

When the LLC cells were incubated with oMCN@DOX@PEG, the cytotoxicity was both dose and time

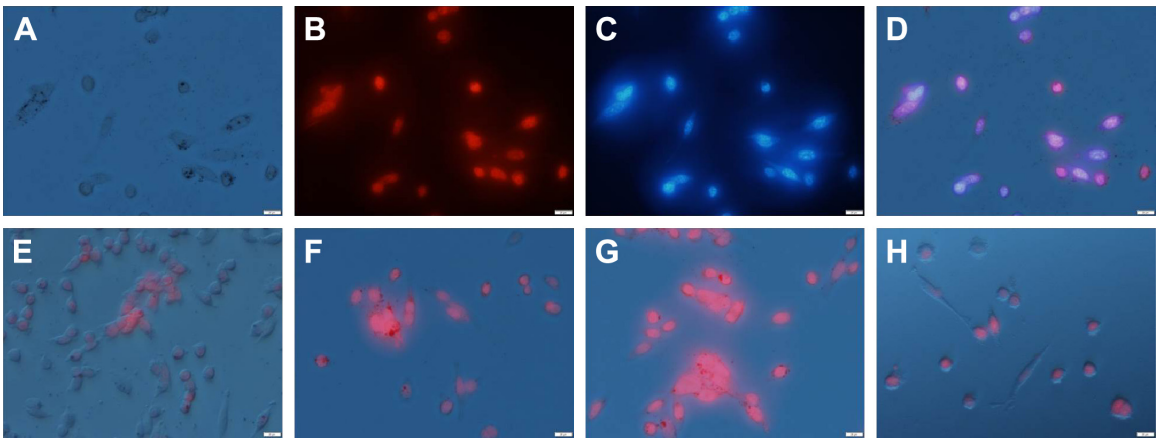

Figure 7 Fluorescent images of LLC cells after co-incubation with 10 μg/mL of oMCN@DOX@PEG at 37°C for 1 h.
Notes: (**A**) Bright-field image, (**B**) DOX, (**C**) nuclei, and (**D**) merging images. (**E**–**G**) Fluorescent images of LLC cells incubated with oMCN@DOX@PEG with the equivalent DOX concentration (~5 μg/mL calculated by the drug-loading efficiency) taken at 0.5 h, 1 h and 2 h, respectively. (**H**) Fluorescent images of LLC cells incubated with 5 μg/mL of DOX for 1 h; the fluorescence is much weaker than that of **F**. The scale bar is 50 μm.
Abbreviations: LLC, Lewis lung carcinoma; oMCN@DOX@PEG, polyethylene glycol-modified doxorubicin-loaded oxidized mesoporous carbon nanospheres; h, hours; DOX, doxorubicin.

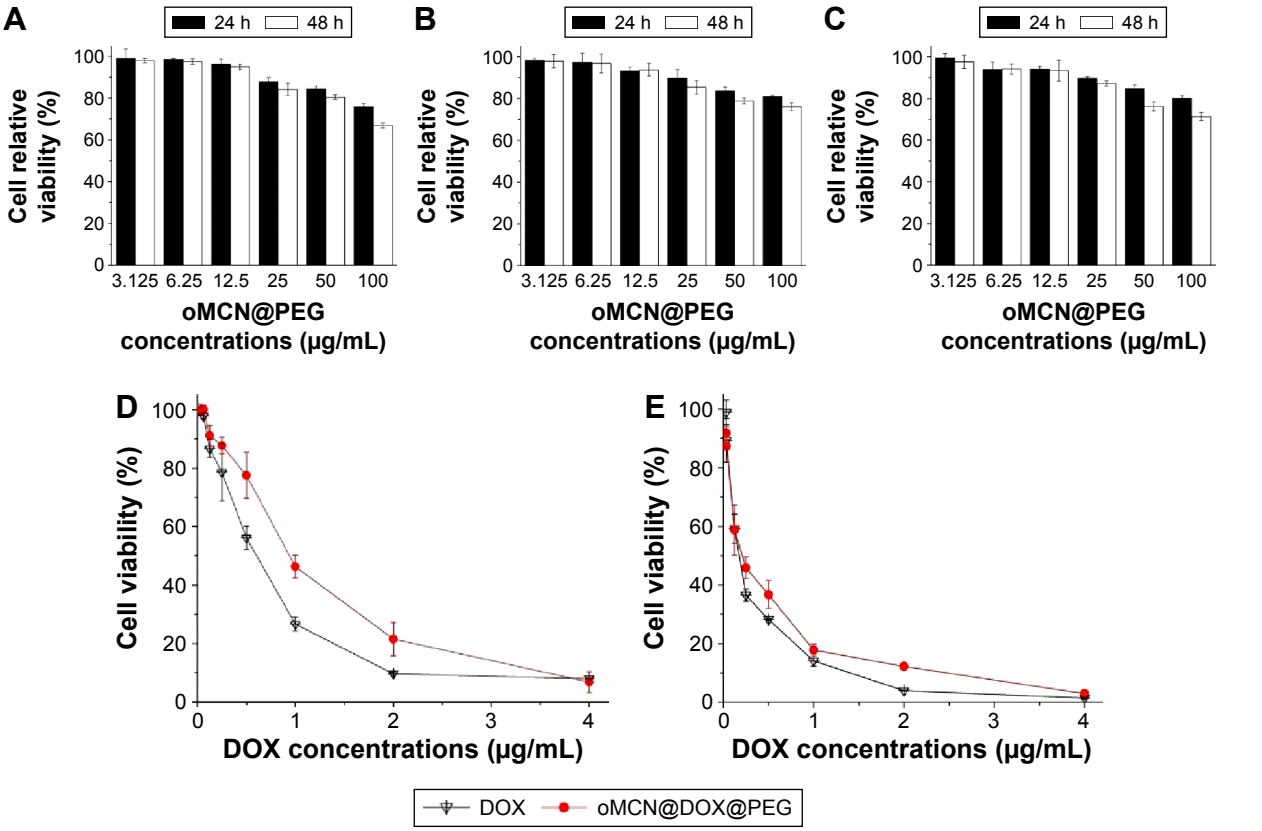

Figure 8 Viability of (**A**) L929, (**B**) Hela, and (**C**) LLC cells after 24 h or 48 h of incubation with different concentrations of oMCN@PEG. Cytotoxicity of LLC cells incubated with free DOX and oMCN@DOX@PEG after (**D**) 24 h and (**E**) 48 h.

Abbreviations: L929, fibroblast line 929; LLC, Lewis lung carcinoma; h, hours; oMCN@PEG, polyethylene glycol-modified oxidized mesoporous carbon nanospheres; DOX, doxorubicin; oMCN@DOX@PEG, polyethylene glycol-modified doxorubicin-loaded oxidized mesoporous carbon nanospheres.

dependent as shown in Figure 8D and E. After 24 hours, ~93% of the cells were killed at the highest concentration (the loaded DOX was 4 μg/mL) and the inhibition ratio reached 97% after 48 hours. The cytotoxicity of DOX stacked on the oMCN@PEG was slightly lower than that of free DOX after incubation for 24 hours as a result of sustained and partial release of DOX from oMCN@PEG. However, after 48 hours, the cytotoxicity showed no significant difference ($P>0.05$). This phenomenon may be due to the effective uptake by tumor cells with the assistance of oMCN@PEG as transmembrane carriers.

Apoptosis of LLC cells

The results of LLC cells apoptosis revealed that oMCN@DOX@PEG induced AnnexinV$^+$/PI$^+$ apoptosis of LLC cells in a dose-dependent manner (Figure 9). The apoptosis effect induced by oMCN@PEG was further studied, and no obvious apoptosis was observed toward LLC cells at three different concentrations, which indicated that the apoptosis induced by oMCN@PEG@DOX was due to DOX released in cells.

Pharmacokinetics

The pharmacokinetic profiles of free DOX, oMCN@DOX, and oMCN@DOX@PEG nanoparticles are shown in Figure 10. Only oMCN@DOX@PEG showed some increase in the concentrations of DOX in plasma compared with those of free DOX or oMCN@DOX. The pharmacokinetic parameters were calculated using noncompartmental model (Table 2). Plasma half-life ($t_{1/2}$) of DOX in oMCN@DOX@PEG formulation was significantly more than that of the free DOX groups ($P<0.05$), and the clearance decreased by >1.68-fold compared with that of free DOX ($P<0.05$). By comparison, the clearance of DOX in oMCN@DOX formulation showed some increase compared with that of free DOX because the oMCN@DOX nanoparticles might be easily recognized by the reticuloendothelial system and rapidly cleared in plasma without PEGylated outer layer. The volume of distribution (V) was calculated to reflect the theoretical volume when the DOX was evenly distributed after injection. The increased V for oMCN@DOX formulation implied decreased concentration of DOX in plasma. As expected, the area under the curve for the oMCN@DOX@PEG formulation was 1.61-fold and

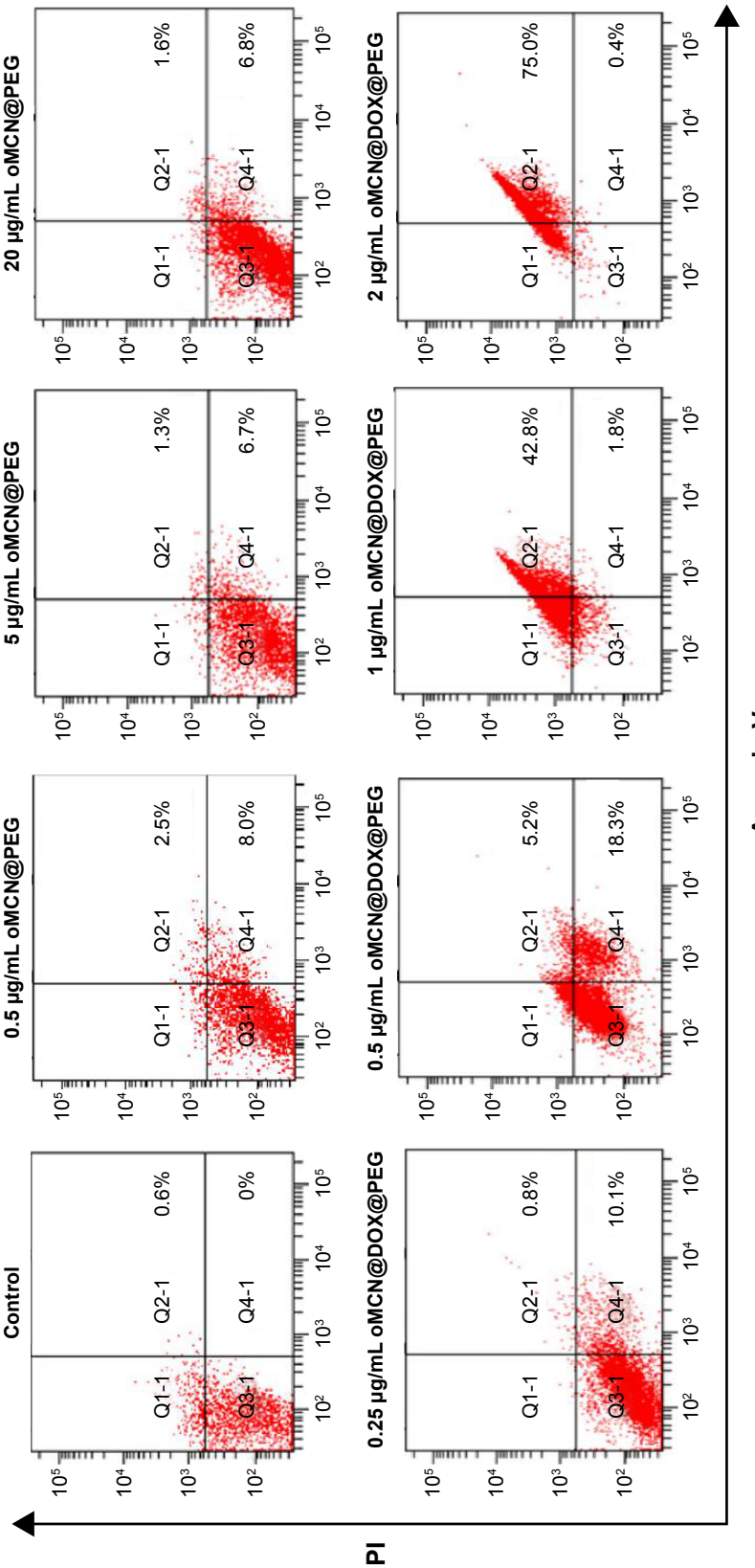

Figure 9 Apoptosis of LLC cells induced by oMCN@PEG and oMCN@DOX@PEG.
Notes: LLC cells were stimulated with 0.5 μg/mL, 5 μg/mL, and 20 μg/mL of oMCN@PEG and 0.25 μg/mL, 0.5 μg/mL, 1 μg/mL, and 2 μg/mL of oMCN@PEG@DOX for 12 h. Apoptosis was then quantified by FACS after staining with Annexin V and PI. The results are presented as fold changes compared with corresponding control cells.
Abbreviations: LLC, Lewis lung carcinoma; oMCN@PEG, polyethylene glycol-modified oxidized mesoporous carbon nanospheres; oMCN@DOX@PEG, polyethylene glycol-modified doxorubicin-loaded oxidized mesoporous carbon nanospheres; h, hours; FACS, fluorescence-activated cell sorter; PI, propidium iodide.

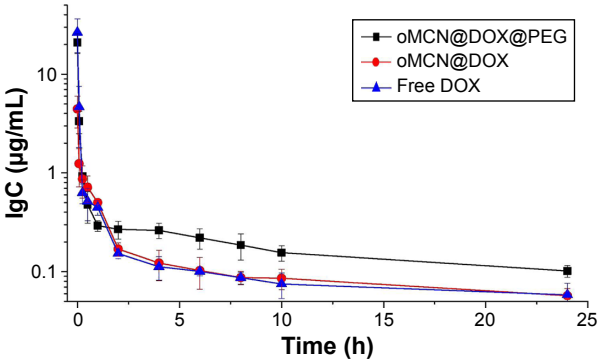

Figure 10 Mean plasma concentration of DOX after iv injection of free DOX, oMCN@DOX, or oMCN@DOX@PEG to Sprague Dawley rats via tail vein at a dose of 8 mg/kg (n=6).
Abbreviations: DOX, doxorubicin; iv, intravenous; oMCN@DOX, doxorubicin-loaded oxidized mesoporous carbon nanospheres; oMCN@DOX@PEG, polyethylene glycol-modified doxorubicin-loaded oxidized mesoporous carbon nanosphere; h, hours; lg C, logarithm of concentration.

1.96-fold higher than that of the free DOX and oMCN@DOX, respectively. In conclusion, the oMCN@DOX@PEG could prolong the circulation of DOX in plasma.

Antitumor effect in vivo

In order to demonstrate the antitumor effect of the delivery system in vivo, free DOX, oMCN@DOX@PEG, and saline were administered into LLC tumor-bearing C57BL/6N mice by injecting via the tail vein and the dose of DOX was 2.5 mg/kg for each mouse. On day 21 after treatment, as shown in Figure 11A, the tumor volume in the mice treated with oMCN@DOX@PEG was 2,394±417 mm^3, showing a 58% decrease ($P<0.01$) compared to that of saline group (5,712±648 mm^3), while free DOX group showed a 60% decrease of the tumor volume (2,279±405 mm^3, $P<0.01$). Although there was no significant superiority in tumor volume decreasing compared to that of DOX, the treatment with oMCN@DOX@PEG significantly extended survival time of tumor-bearing mice (Figure 11B). The mean survival time of the mice injected with saline was 25±1.2 days (23–26 days). Mice treated with oMCN@DOX@PEG showed a longer survival time (30±3.2 days, $P<0.01$), followed by the DOX treatment group (27±2.6 days, $P>0.05$). It is worth noting that the remarkable body weight loss of mice in the DOX treatment group suggested that systemic toxicity had been induced by the administration of free DOX (Figure 11C). Unlike the free DOX treatment group, the body weight of mice in the oMCN@DOX@PEG treatment group did not show obvious decrease, implying that being vehicles for DOX, the delivery system based on oMCN@PEG can effectively reduce the toxicity effects of DOX as expected in drug-releasing behavior in vitro (Figure 6F).

Table 2 Pharmacokinetic parameters of DOX after iv injection of free DOX, oMCN@DOX, or oMCN@DOX@PEG to Sprague Dawley rats via tail vein

Parameters	Formulations		
	Free DOX	oMCN@DOX	oMCN@DOX@PEG
$t_{1/2}$ (h)	11.24±5.58	19.10±10.41	22.29±5.81[a]
CL (L/h/kg)	1.53±0.30	1.83±0.44	0.91±0.09[b,c]
V (L/kg)	24.19±12.28	46.29±21.27[a]	28.97±6.84
$AUC_{0-\infty}$ (mg/L/h)	5.48±1.45	4.52±0.85	8.84±0.84[b,c]

Notes: Data are expressed as mean ± SD (n=6). [a]$P<0.05$ vs free DOX. [b]$P<0.01$ vs free DOX. [c]$P<0.01$ vs oMCN@DOX.
Abbreviations: DOX, doxorubicin; iv, intravenous; oMCN@DOX, doxorubicin-loaded oxidized mesoporous carbon nanospheres; oMCN@DOX@PEG, polyethylene glycol-modified doxorubicin-loaded oxidized mesoporous carbon nanospheres; $t_{1/2}$, plasma half-life; h, hour; CL, clearance; *V*, volume of distribution; AUC, area under the curve; SD, standard deviation.

The metastasis of advanced malignant cancer is one of the main causes leading to death. In order to observe the pulmonary metastasis of all the tumor-bearing mice, the lungs from each group were removed to count the tumor metastasis nodules. As it is clearly shown in Figure 11E, there were a large number of surface metastatic tumor nodules for the saline treatment group, followed by the free DOX treatment group, and the number rose rapidly as time increased. Few metastatic tumor nodules could be seen on the surface of lungs in the oMCN@DOX@PEG treatment group. The significant metastasis inhibition effect of oMCN@DOX@PEG accounted for the improved survival time of tumor-bearing mice.

The ex vivo fluorescent images of excised organs and tumors as shown in Figure 11F clearly confirmed the distribution of the drugs. The free DOX molecules mainly accumulated in metabolic organs, particularly in liver. However, oMCN@DOX@PEG changed the distribution of DOX molecules. Many studies have demonstrated that the PEGylation of nanoparticles is one of the most efficient ways to enhance the blood circulation and enhanced permeability and retention effect as well as to prevent their uptake by hepatic macrophages.[25–27] The presence of enhanced permeability and retention effect makes nanoparticles accumulate in the tumor tissue. Typically, the agglomerated nanoparticles tend to accumulate efficiently into the lung during circulation of blood inhibiting tumor metastasis.[28,29]

Conclusion

A DDS based on PEGylated oxidized mesoporous carbon nanospheres (oMCN@PEG) has been successfully fabricated in a facile strategy. Such a nanoplatform integrates the advantages of well-defined morphology, suitable diameter, excellent hydrophilicity, good biocompatibility, and high

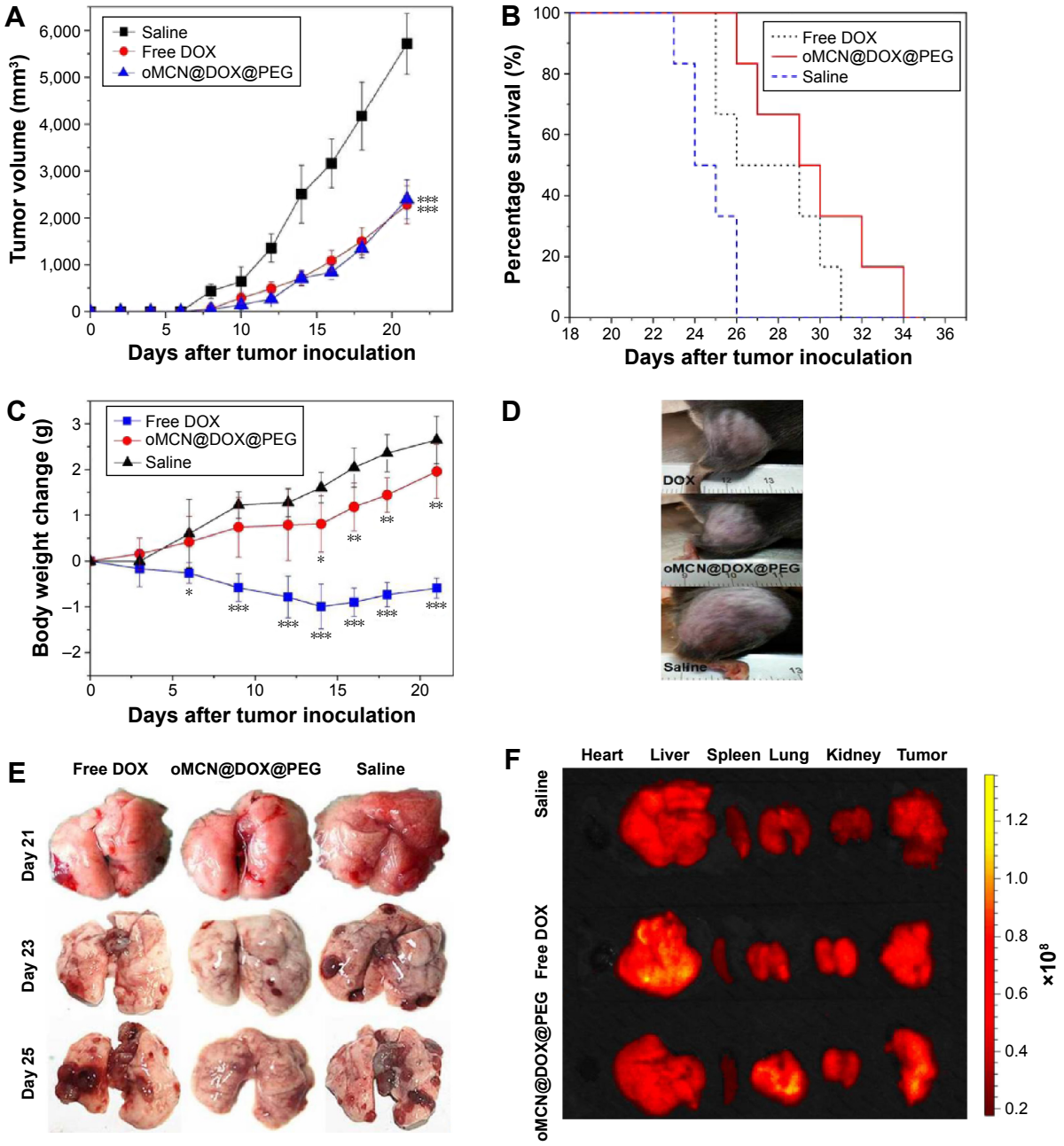

Figure 11 In vivo therapy of free DOX, oMCN@DOX@PEG, and saline on LLC model.

Notes: (**A**) The growth curves of primary tumor; (**B**) survival time curves, (**C**) body weight, and (**D**) typical photos of tumor size in the right hind legs of C57BL/6N mice bearing LLC treated with free DOX, oMCN@DOX@PEG (2.5 mg/kg), and saline. Six mice per group were used. Data are presented as mean ± SD. (**E**) Lungs from the tumor-bearing mice treated with free DOX, oMCN@DOX@PEG, and saline were removed and visually examined for the number of metastatic tumor nodules on days 21, 23, and 25. (**F**) Ex vivo fluorescence images of excised organs and tumors at 12 h post injection of the formulations. *$P<0.05$ vs saline, **$P<0.01$ vs saline, and ***$P<0.001$ vs saline (n=6).

Abbreviations: DOX, doxorubicin; oMCN@DOX@PEG, polyethylene glycol-modified doxorubicin-loaded oxidized mesoporous carbon nanospheres; LLC, Lewis lung carcinoma; SD, standard deviation.

payload of DOX. The pH-dependent drug loading and release from oMCNs was successfully achieved. The drug system (oMCN@DOX@PEG) exhibited excellent stability under neutral pH conditions while releasing DOX in acidic conditions such as tumor environment. Pharmacokinetics study revealed that oMCN@DOX@PEG could prolong the circulation of DOX in the blood. This carbonaceous nanoparticle material could efficiently penetrate the membrane of tumor cells and subsequently release drugs in the cancer cells in a pH-dependent manner, inhibiting growth and inducing apoptosis of LLC cells with minimal toxicity and side effect of DOX. Most importantly, oMCN@DOX@PEG exhibited significant therapeutic effect and enhanced antimetastasis effect against cancer cells in vivo. In view

of the simple fabrication process of oMCN@DOX@PEG and their outstanding performances in anticancer therapy, it is expected to lead to further development for a variety of biotechnological and biomedical applications.

Acknowledgment

This work was financially supported by a grant from the National Natural Science Foundation of China (21401214) and a youth startup foundation grant from Second Military Medical University (2013QN03).

Disclosure

The author reports no conflicts of interest in this work.

References

1. Tang F, Li L, Chen D. Mesoporous silica nanoparticles: synthesis, biocompatibility and drug delivery. *Adv Mater*. 2012;24(12):1504–1534.
2. Chen Y, Chen HR, Shi JL. Construction of homogenous/heterogeneous hollow mesoporous silica nanostructures by silica-etching chemistry: principles, synthesis, and applications. *Acc Chem Res*. 2014;47(1):125–137.
3. Li X, Xie QR, Zhang J, Xia W, Gu H. The packaging of siRNA within the mesoporous structure of silica nanoparticles. *Biomaterials*. 2011;32(35):9546–9556.
4. Chen Y, Xu P, Wu M, et al. Colloidal RBC-shaped, hydrophilic, and hollow mesoporous carbon nanocapsules for highly efficient biomedical engineering. *Adv Mater*. 2014;26(25):4294–4301.
5. Wang C, Xu H, Liang C, et al. Iron oxide @ polypyrrole nanoparticles as a multifunctional drug carrier for remotely controlled cancer therapy with synergistic antitumor effect. *ACS Nano*. 2013;7(8):6782–6795.
6. Kim TW, Chung PW, Slowing II, Tsunoda M, Yeung ES, Lin VS. Structurally ordered mesoporous carbon nanoparticles as transmembrane delivery vehicle in human cancer cells. *Nano Lett*. 2008;8(11):3724–3727.
7. Zhu J, Liao L, Bian X, Kong J, Yang P, Liu B. pH-controlled delivery of doxorubicin to cancer cells, based on small mesoporous carbon nanospheres. *Small*. 2012;8(17):2715–2720.
8. Niu X, Wan L, Hou Z, et al. Mesoporous carbon as a novel drug carrier of fenofibrate for enhancement of the dissolution and oral bioavailability. *Int J Pharm*. 2013;452(1–2):382–389.
9. Miao P, Tang YG, Kun H, Wang BD. Facile synthesis of carbon nanodots from ethanol and their application in ferric(III) ion assay. *J Mater Chem A*. 2015;3:15068–15073.
10. Zhi X, Fang H, Bao C, et al. The immunotoxicity of graphene oxides and the effect of PVP-coating. *Biomaterials*. 2013;34(21):5254–5261.
11. Pondman KM, Sobik M, Nayak A, et al. Complement activation by carbon nanotubes and its influence on the phagocytosis and cytokine response by macrophages. *Nanomedicine*. 2014;10(6):1287–1299.
12. Fang Y, Gu D, Zou Y, et al. A low-concentration hydrothermal synthesis of biocompatible ordered mesoporous carbon nanospheres with tunable and uniform size. *Angew Chem Int Ed*. 2010;49(43):7987–7991.
13. Sanchez-Sanchez A, Suarez-Garcia F, Martinez-Alonso A, Tascon JMD. Surface modification of nanocast ordered mesoporous carbons through a wet oxidation method. *Carbon N Y*. 2013;62:193–203.
14. Wu Z, Webley PA, Zhao D. Comprehensive study of pore evolution, mesostructural stability, and simultaneous surface functionalization of ordered mesoporous carbon (FDU-15) by wet oxidation as a promising adsorbent. *Langmuir*. 2010;26(12):10277–10286.
15. Jung SH, Jung SH, Seong H, Cho SH, Jeong K, Shin BC. Polyethylene glycol-complexed cationic liposome for enhanced cellular uptake and anticancer activity. *Int J Pharm*. 2009;382(1–2):254–261.
16. Ishak RAH, Awad GAS, Zaki NM, El-Shamy AEA, Mortada ND. A comparative study of chitosan shielding effect on nano-carriers hydrophilicity and biodistribution. *Carbohydr Polym*. 2013;94(1):669–676.
17. Ma LL, Jie P, Venkatraman SS. Block copolymer 'stealth' nanoparticles for chemotherapy: interactions with blood cells in vitro. *Adv Funct Mater*. 2008;18(5):716–725.
18. Yang X, Zhang X, Liu Z, Ma Y, Huang Y, Chen Y. High-efficiency loading and controlled release of doxorubicin hydrochloride on graphene oxide. *J Phys Chem C*. 2008;112(45):17554–17558.
19. Yang W, Yu S, Chen S, Liu Y, Shao Z, Chen X. Doxorubicin-loaded silk fibroin nanospheres. *Acta Chim Sin*. 2014;72(11):1164–1168.
20. Niu C, Wang Z, Lu G, et al. Doxorubicin loaded superparamagnetic PLGA-iron oxide multifunctional microbubbles for dual-mode US/MR imaging and therapy of metastasis in lymph nodes. *Biomaterials*. 2013;34(9):2307–2317.
21. Tian Y, Li S, Song J, et al. A doxorubicin delivery platform using engineered natural membrane vesicle exosomes for targeted tumor therapy. *Biomaterials*. 2014;35(7):2383–2390.
22. Qian H, Wang X, Yuan K, et al. Delivery of doxorubicin in vitro and in vivo using bio-reductive cellulose nanogels. *Biomater Sci*. 2014;2(2):220–232.
23. Guan X, Li Y, Jiao Z, et al. A pH-sensitive charge-conversion system for doxorubicin delivery. *Acta Biomater*. 2013;9(8):7672–7678.
24. Al-Husari M, Webb SD. Regulation of tumour intracellular pH: a mathematical model examining the interplay between H+ and lactate. *J Theor Biol*. 2013;322:58–71.
25. Bai J, Zhou Z, Tang H, Song S, Peng J, Xu Y. Impact of PEGylation on biodistribution and tumor accumulation of lipid-Mu peptide-DNA. *J Liposome Res*. 2013;23(1):1–10.
26. Mei L, Fu L, Shi K, et al. Increased tumor targeted delivery using a multistage liposome system functionalized with RGD, TAT and cleavable PEG. *Int J Pharm*. 2014;468(1–2):26–38.
27. Ishida T, Ichihara M, Wang X, et al. Injection of PEGylated liposomes in rats elicits PEG-specific IgM, which is responsible for rapid elimination of a second dose of PEGylated liposomes. *J Control Release*. 2006;112(1):15–25.
28. Key J, Kim YS, Tatulli F, et al. Opportunities for nanotheranosis in lung cancer and pulmonary metastasis. *Clin Transl Imaging*. 2014;2(5):427–437.
29. Xu P, Yin Q, Shen J, et al. Synergistic inhibition of breast cancer metastasis by silibinin-loaded lipid nanoparticles containing TPGS. *Int J Pharm*. 2013;454(1):21–30.